



LAWRENCE
LIVERMORE
NATIONAL
LABORATORY

Diamond machining of ZnSe gratings for the Near Infrared Imager and Slitless Spectrograph (NIRISS) onboard JWST

P. J. Kuzmenko, S. L. Little, L. Albert, D. A. Aldridge, R. Doyon, M. Maszkiewicz, D. Touahri

May 20, 2014

Advances in Optical and Mechanical Technologies for
Telescopes and Instrumentation
Montreal, Canada
June 22, 2014 through June 27, 2014

Disclaimer

This document was prepared as an account of work sponsored by an agency of the United States government. Neither the United States government nor Lawrence Livermore National Security, LLC, nor any of their employees makes any warranty, expressed or implied, or assumes any legal liability or responsibility for the accuracy, completeness, or usefulness of any information, apparatus, product, or process disclosed, or represents that its use would not infringe privately owned rights. Reference herein to any specific commercial product, process, or service by trade name, trademark, manufacturer, or otherwise does not necessarily constitute or imply its endorsement, recommendation, or favoring by the United States government or Lawrence Livermore National Security, LLC. The views and opinions of authors expressed herein do not necessarily state or reflect those of the United States government or Lawrence Livermore National Security, LLC, and shall not be used for advertising or product endorsement purposes.

Diamond machining of ZnSe grisms for the Near Infrared Imager and Slitless Spectrograph (NIRISS) onboard JWST

Paul J. Kuzmenko^{*a}, Steve L. Little^a, Loïc Albert^b, David A. Aldridge^c,
René Doyon^b, Michael Maszkiewicz^d, and Driss Touahri^c

^aLawrence Livermore National Laboratory, L-183 PO Box 808, Livermore, CA 94551;

^bUniversité de Montréal, Département de Physique, Montréal, QC H3T 1J4, Canada;

^cCOMDEV International Ltd., 303 Terry Fox Dr., Kanata, ON K2K 3J1, Canada;

^dCanadian Space Agency, 6767 Route de l'Aéroport, Saint-Hubert, QC J3Y 8Y9, Canada

ABSTRACT

LLNL diamond machined a ZnSe grism for spectroscopy of transiting exoplanets on NIRISS, a Canadian instrument that will fly on the James Webb Space Telescope. The grism operates over the wavelength range of 0.6 to 2.5 μm . It is cross-dispersed by a ZnS prism and has a resolving power in first order of ~ 700 . The surface error over the full 29 x 30 mm grating aperture is 0.03 wave rms at 633nm. We measured a diffraction efficiency at 633 nm of 56% (nearly 88% after accounting for Fresnel reflection). The diffraction pattern is clean with no discernible ghosts.

Keywords: grism, NIRISS, JWST, diamond machining, immersion grating, near infrared, ZnSe,

1. INTRODUCTION

The James Webb Space Telescope (JWST) is an international collaborative effort. The Canadian Space Agency (CSA) contribution is the Fine Guidance Sensor (FGS), which works with the JWST attitude control system to provide highly accurate pointing. In addition the FGS contains the science module NIRISS (Near Infrared Imager and Slitless Spectrograph). NIRISS is a multi-functional instrument capable of wide field grism spectroscopy, single object grism spectroscopy, aperture masking interferometry and broad-band imaging^{1,2}. It incorporates a Teledyne HAWAII-2RG 2048 x 2048 pixel HgCdTe array with a 5.3 μm cutoff as well as a pupil wheel and a filter wheel.

The single object slitless spectroscopy (SOSS) observing mode of NIRISS is optimized to perform spectroscopy on transiting exoplanets³. This requires moderate spectral resolution over the wavelength range of 0.6 to 2.5 μm . The GR700XD (shown in figure 1), consisting of a ZnSe grism and a ZnS cross-dispersing prism, provides the spectral dispersion. Grism orders 1 and 2 cover the desired wavelength range. A peak resolving power of ~ 700 is required at the blaze wavelength of 1.23 μm .

On the basis of prior experience in machining gratings in brittle optical materials^{4,5}, LLNL was asked to fabricate the ZnSe grism for the GR700XD. This paper will describe the efforts that led to the successful realization of a grism for NIRISS and some lessons learned along the way. Section 2 lists the grism specifications and details the challenges anticipated in meeting them. It was important to qualify the machine performance and diamond tools before cutting flight gratings. These efforts are described in section 3. Details of the grism fabrication are given in section 4. Section 5 covers testing of grism #1 at LLNL and a comparison of measured and modeled diffraction efficiency. Section 6 describes fabrication and testing of grism #2 and notes the effect of spindle feed direction on groove quality. Conclusions and future work are discussed in section 7.

2. NIRISS GR700XD GRISM SPECIFICATIONS

The original NIRISS optical design called for a KRS-5 (thallium bromoiodide) grism. LLNL had no experience diamond machining KRS-5 and it is a very toxic material. A request was made to substitute ZnSe, which has a comparable

*kuzmenko1@llnl.gov; phone 925-423-4346; fax 925-422-2499

refractive index, good transmission over the wavelength range of interest, and can be diamond-machined. A rework of the optical design showed that a ZnSe grism was an acceptable substitute and produced the following specifications:

ZnSe grism Specifications

1. Grating density: 54.3 lines/mm \pm 0.2 lines/mm
2. Facet blaze angle: 2.63 degrees \pm 0.20 degrees
3. Prism apex angle: 1.9 \pm 0.1 degrees
4. Clear aperture: It should be as large as possible on the recessed 29x30mm surface. The field mask is about 28x29mm.
5. Grating surface error: $\lambda/3$ at 633 nm peak-to-valley (PV) across the clear aperture, with a goal of $\lambda/5$.
6. Rms grating surface error: $\lambda/12$ with a goal of $\lambda/20$ at 633 nm. This assumes surface error behaves like spherical aberration alone with a scale factor of 4 between rms and PV.
7. Diffraction efficiency: The peak of the blaze function should be 60% with a goal of 70% efficiency in order 1 at $1.23 \pm 0.10 \mu\text{m}$. This efficiency includes only the grating contribution, not the Fresnel reflection losses or the bulk throughput of the substrate.
8. Light scattering: When uniformly illuminated by a HeNe laser, the intensity of light scattered between any pair of orders should be $< 1\%$ of the integrated peak of the brightest order. It is acceptable that the total scattered light (integrated over all spectral positions) be $> 1\%$.
9. Ghosts: When uniformly illuminated by a HeNe laser, peak ghost intensity should remain at a level $< 1\%$ of the integrated peak of the brightest order.

Figure 2 shows a drawing of the grism blank with detail of the grating surface. The optical surfaces of the blank are specified to be flat to $\lambda/4$ over the full aperture with a scratch & dig of 60/40 or better.

We anticipated challenges in meeting these some of these specifications. The largest grisms previously machined at LLNL that would have met the GR700 surface error specification⁴ had only $1/4$ of the grooved area of the NIRISS grism. These earlier grisms operated in the MWIR where the tolerances on scatter due to surface roughness and random groove position error are less severe. Ghost intensity as a function of periodic groove error⁶ scales as $1/\lambda^2$. This requirement also becomes more difficult to achieve at shorter wavelengths.

Zinc selenide brings its own machining issues. It is weaker than more common infrared materials such as silicon and germanium. Without careful preparation to remove all subsurface damage created during the grinding and polishing of the blank, grooves are very prone to chip during the machining process⁵. Subsurface damage on the sides of the substrate as opposed to the optical surface can produce increased chipping and surface error near the edges of the grating. This causes concern when the clear aperture is specified to cover a very large fraction of the physical grating.

The estimated machining time was nearly 6 days, which could not be interrupted by AC power glitches, significant seismic events, or large changes in barometric pressure (the laser interferometer that performs machine metrology is not pressure compensated). Our approach to all these potential difficulties was to tightly control the machining conditions and the substrate surface as much as possible. For example the temperature of the machine enclosure was stabilized to $\pm 0.02^\circ\text{F}$ and that of the machine room to $\pm 0.25^\circ\text{F}$.

3. MACHINE QUALIFICATION AND CUTTING TEST GRATINGS

LLNL's Precision Engineering Research Lathe (PERL) had been shut down for several months for electrical safety inspections and repairs. Before attempting to machine a high quality grating we needed to restart the machine and demonstrate that its performance was unchanged. The first step was to power up the thermal control systems for both the machine room and the machine enclosure. After allowing the machine to achieve thermal equilibrium, we monitored temperatures at several locations in and around the machine for a few days to verify that tight thermal control was achieved. The next step was to test the metrology system by comparing a directed motion of one inch with a precision gauge block of the same length. The final step was to test machine stability over a 24 hour period by commanding the spindle to hold position while measuring axial spindle motion with a capacitive sensor. PERL performance was

satisfactory and we prepared to cut a test grating. There is a two-fold purpose in cutting a test grating. Besides being a severe test of machine precision and stability it also allows one to verify the blaze angle cut into the diamond tool.

We chose to cut the first test grating into an etched germanium blank. Previous experience has shown that there is negligible wear of the diamond tool in cutting germanium. The 30° negative rake tool angle that is optimal for cutting grooves in germanium also works well for zinc selenide. Two tools had been ordered for this project with a blaze angle specified to be 2.6°. Unfortunately the test gratings cut with each tool showed very unusual diffraction patterns. Microscope inspection showed that the back edges of the tools were rubbing across the grating surface and destroying the vertical facet of the grooves.

Due to tight time considerations we had to modify an existing diamond tool to proceed. This tool had a blaze angle of 2.89° but, by carefully grinding on the tool shank, it was possible to add a small amount of tilt to the tool in its holder and obtain an effective blaze near 2.6°. We used this modified tool to cut a coarse grating (32 lines/mm) in an etched germanium blank. Coarser grating have diffraction orders more closely spaced in angle, which makes it easier to measure blaze (less interpolation between orders). The blaze angle was measured to be 2.59° using a HeNe laser and a precision rotation stage with 1 arc minute resolution⁷. A scan of the grating surface with an optical profilometer showed a nearly ideal groove shape and a surface roughness of only a few nm on the facets. With good results achieved in germanium the final step before machining the flight gratings was to cut a test grating in ZnSe.

Zinc selenide is a more difficult material to machine for several reasons. Unlike germanium, which can be obtained as a single crystal with an optimal orientation of the crystal axes, optical quality ZnSe is only available in polycrystalline form. It is a softer and weaker material than germanium and more prone to chipping. Finally, good polishing etches have been developed for germanium that remove outer damaged layers in a controlled manner leaving a very smooth damage-free surface to machine. ZnSe etches exist but remove material very non-uniformly. The only alternative to obtain a damage-free surface is very careful polishing. By cutting a test grating in a sample of ZnSe that has received the same polishing treatment as the flight gratings, one can determine whether the surface of the blank is sufficiently damage free for high quality grooves or will need to be redone. BMV Optical Technologies polished the ZnSe blanks for the flight gratings. At the same time and with the same procedures they polished a plane parallel disc of ZnSe (5.6 mm thick and 25.4 mm in diameter) for the test grating. The surfaces were flat to better than $\lambda/5$ peak to valley (PV) @ 633 nm.

The ZnSe disc was fastened to a steel parallel bar with wax as shown in figure 2 and was mounted to the machining stage of PERL. We started the machine spindle, letting it run for 12 hours to establish thermal equilibrium, before starting to cut the grating to JWST specification (18.7 μm period). The spindle was run at 1000 rpm using a feed rate of 0.35 inch per minute. Cutting began with the spindle at minimum extension, moving outward to cut successive grooves.

Previous experiments had shown that Rowland ghosts in gratings machined on PERL can be reduced to imperceptible levels if the grooves are cut unidirectionally⁸. This means, for example, cutting a groove only when the blank is moving left to right and then moving the tool around the blank to cut the next groove while the blank is again moving left to right. The extra machine motion adds about 30 to 40% to the fabrication time but was judged to be a worthwhile benefit for the flight gratings. It was important to demonstrate this on the test grating. Unidirectional feed made it possible to implement climb cutting (i.e. direction of feed motion is same as direction of tool motion while in contact with part), which is known to produce a better surface finish and less tool wear. About 50 hours were required to cut a test grating over half the surface of the ZnSe disc. We believed this to be adequate to validate the cutting process while not incurring excessive wear on the diamond tool.

After machining was completed the ZnSe disc was removed from PERL (see figure 2) and cleaned. Under low power magnification the grating looked good with very little evidence of groove chipping. This confirmed that the ZnSe as polished was free of subsurface damage. An optical profilometer measurement, shown in figure 3, indicates that the groove surfaces are very flat and smooth with an rms roughness of just a few nm. Some distortion seen near the tips appears to be an artifact due to the transparency of the ZnSe.

Since the GR700XD grism operates in transmission, it was useful to examine the diffraction pattern of the test grating in a transmitted beam. We demounted the disc from the steel bar and directed a HeNe beam at approximately normal incidence onto the flat side so that the beam travelled through the ZnSe and exited through the grating surface. The

diffraction pattern was then displayed on a nearby wall. The pattern was very clean with nearly all the diffracted light falling in order 2. All other nearby orders were quite dim, in agreement with theoretical predictions of grism performance. No ghosts were visible between orders. Minimal scatter was observed between the diffraction orders.

We set up a rotary stage and a He Ne laser as with the germanium test grating. The blaze angle of the ZnSe test grating was determined to be 2.72° .

Surface error is a key specification in determining grism performance so the ZnSe test grating was set up in a Zygo interferometer for measurement in reflection. The full aperture surface error of the test grating was 0.161 wave PV and 0.026 wave rms. Stopping the aperture down to 80% reduced the surface error to 0.104 wave PV and 0.019 wave rms. There is some excess surface error near the edges as can be seen from figure 4. However, the ZnSe test ruling met the GR700XD specifications given in section 2. A decision was made to proceed with the machining of the flight grisms.

4. GRISM #1 FABRICATION

Unlike the ZnSe disc used for the test grating, the grism has a complex shape with compound angles. So a special machining fixture is needed to rigidly support the blank in the proper orientation during the machining process. We chose to make the fixture of mild steel to match the CTE of PERL's mechanical structure. This minimizes relative motion between the tool and the blank in the presence of small drifts in temperature and is very important since there is no active control of the vertical position of the tool.

Our fixture is a scaled up version of one used to machine germanium grisms⁴. It is relatively thin so that the blank rests at a low enough height to allow an adequate radius of rotation of the diamond tool. The grism blank rests on 3 mounting pads, which are 2 mm x 2 mm, and are positioned near the edge of the clear aperture. Metal pins constrain the blank laterally. The heights of the pads are set to accommodate the compound angle on the entrance face and to produce the desired apex angle when the grating is machined into the upper surface of the blank. Three fine-pitch (40 TPI) jacking screws permit the top of the fixture to be leveled very precisely. Details of the fixture may be seen in figure 6.

As previously described⁴ the grism blank is secured to the fixture mounting pads using a cyanoacrylate adhesive. It is very important that the blank be mounted as stress-free as possible. We hold the blank with a special 3 pin fixture while it is being lowered onto the mounting pads so downward force is applied only to points directly above the pads. The gluing of the blank to the holding fixture and to the machining fixture is done in a controlled environment held at the same temperature as the machine enclosure. This ensures that there is minimal temperature change and therefore minimal thermally induced stress due to the CTE mismatch between the blank and the fixture when the fixture is installed in PERL. The cyanoacrylate is left to cure overnight to maximize chemical resistance. Exposure to the odorless mineral oil used as a coolant and cutting fluid can loosen the adhesive bonds if not fully cured. Next the mounting fixture with is bolted to the PERL translation stage. Special indicator gauges are used to level the top of the fixture and to align the edges of the fixture to the machine axes to within one micron over the range of travel of the machining.

Once it is verified that the temperature of the room and the temperature inside the PERL machine enclosure are stable the machine spindle is started. We also begin the mineral oil spray onto the ZnSe blank at this time. The spindle motor provides an additional heat source inside the machine enclosure. It is necessary to wait about 12 hours after the motor starts for the temperature of the machine and its enclosure to stabilize. The numerical control program holds the rotating tool away from the blank during this thermal soak time. Then the cutting of the grooves commences.

The cutting parameters were the same as the ZnSe test grating. We used a spindle speed of 1000 rpm and a feed rate of the translation stage of 0.35 inch/minute. The grooves were cut in a unidirectional manner using climb cutting. One difference is that the spindle was nearly fully extended when the cutting began and moved inward to cut successive grooves. This is the opposite of what was done in cutting the test grating.

The rationale for having the spindle move inward during the duration of the cutting is based on the predicted long machining time and the fact that the laser interferometer controlling PERL does not compensate for changes in atmospheric pressure. It simply measures changes in the optical path by counting interference fringes and cannot

distinguish between changes in physical path length and the fringe shifts caused by changes in the refractive index along that path.

Each axis of PERL uses a Michelson interferometer with one arm of fixed length 2.5 cm. The other arm of the interferometer has a corner cube reflector mounted on a moving stage. The path length of the moving arm can vary from 2.5 to 10 cm over its full range of travel. The greater the difference in length between the fixed and moving paths the greater the effect of pressure changes. If we assume that the trend of atmospheric pressure is a random walk (i.e. ΔP increases with time) then the effect of pressure drift is somewhat mitigated by reducing the difference in optical path between the interferometer arms as machining proceeds (i.e. have spindle move inward as it cuts successive grooves).

Once started the machining took 136 hours to complete, then the fixture was removed from the machine. There was quite a bit of ZnSe particulate residue mixed with mineral oil on the part as can be seen in figure 6. To clean the grism we flushed the surface with isopropyl alcohol and gently pushed the particles out the grooves with an artist's brush. This was followed by a final flush with alcohol, and a stream of clean moisture-free nitrogen to dry the grooves. Grism #1 was now ready for testing.

5. GRISM #1 TESTING AND EFFICIENCY MODELING

The first step after the initial cleaning was to inspect the machined surface under a microscope and take photographs. A small amount of subsurface damage could be seen but the overall quality was good. Some particulate residue remained so the grism was cleaned again with a strippable coating. Next a 3 x 3 grid pattern was set up across the grism surface. Microscope photographs and optical profilometry measurements were taken at each point. Figure 7 shows the profilometry data from the center of the grism. While still mounted in its fixture the grism blaze angle was measured to be 2.55°.

Surface error was measured with a Zygo interferometer both before and after the grism was removed from the machining fixture. A very small increase in wavefront error (0.013 wave P-V over the full aperture) after the grism was demounted indicated that the blank was slightly stressed while mounting or that the cyanoacrylate cured with the fixture at a slightly different temperature than that of the machine enclosure. The measurement showed a surface error over the full grating surface of 0.209 wave P-V, 0.030 wave rms and 0.125 wave P-V, 0.022 wave rms over the central 80% of the aperture. Figure 8 shows the 2D and 3D representations of the surface error.

A simple but very informative test is to pass a He laser beam through the grism and then examine the diffraction pattern. A good grating gives clean, sharp diffracted spots with power concentrated in one or two orders near the blaze direction. Figure 9 shows that grism #1 produces a very clean diffraction pattern with nearly all the power going into a second order spot at 633 nm. Furthermore no grating ghosts are visible and nor is there scattered light appearing between the orders.

To obtain a quantitative measurement of the diffraction efficiency we adjusted the configuration slightly to simulate the optical path in NIRISS. The grism rested as shown in figure 1 with the grooves running horizontally. We oriented a vertically polarized HeNe beam to strike the entrance face at a 17° angle of incidence, the same as in the GR700XD. The incident laser power measured 1.20 mW with a reflection of 0.25 mW from the entrance face. The measured reflectivity of 20.8% matches the reflectivity of 21.0% calculated using the Fresnel equations and a refractive index⁹ of 2.592 for ZnSe at 633 nm and 293 K. This helps validate the technique.

The power in the brightest transmitted order measured 0.67 mW, giving a diffraction efficiency in 2nd order of 56%. If we subtract from the incident power the power reflected at the entrance face (to simulate an ideal AR coating), the diffraction efficiency increases to nearly 71%. The orders on either side of the bright order measured 3.6 microwatt and 0.3 microwatt, indicating that 633 nm is very near the peak of the blaze.

We repeated this measurement using a polarized diode laser at 1534 nm. But with only a fluorescent card to locate the infrared beams and a small area (2 mm x 2 mm) detector we measured anomalously low values for the entrance face reflectivity (14% vs. calculated values of 16.5% to 19% depending on polarization). Most likely the detector was not

capturing the full beam and we could only put a lower bound on the diffraction efficiency at 1534 nm of 40%.

Although the diffraction efficiency over the entire 0.6 to 2.5 μm range of operation is of interest, lasers only provide data at a single wavelength. So we turned to electromagnetic modeling of the grism to fill in the gaps. PCGrate is a software application that calculates the diffraction efficiency of one-dimensional gratings using the rigorous boundary integral equation method. The input for PCGrate is the groove profile and the material properties. Consider the Y-profile shown in figure 7. There are four complete grooves traced out along that profile. Each of them was used in a separate PCGrate calculation resulting in four separate diffraction efficiency curves. This procedure was followed at 4 of the 9 sample points on grism #1 at which profilometer data was taken yielding in 16 efficiency curves. These curves were averaged to produce the composite efficiency curve shown in figure 10. The experimental measurement at 633 nm is plotted as well.

6. GRISM #2 FABRICATION AND TESTING

We were very satisfied with the optical performance of grism #1. The diffraction efficiency and surface error were both excellent. Since LLNL was contracted to deliver 2 grisms a second one would be machined using similar procedures. However, as can be seen in figure 11, chipping of the vertical faces and groove corners was noticeably worse in grism #1 than in the test grating. There are several possible explanations. Accumulating wear of the diamond tool could make the surface of grism #1, which was cut at a later date, of poorer quality than the test grating. It is possible that the test blank and the grism blank were polished differently and had differing degrees of subsurface damage prior to machining. It is also possible that the difference in the direction of the spindle feed in cutting successive rows has an effect.

To test this latter hypothesis we machined two small area gratings on the unused half of the ZnSe test grating blank using opposite directions of spindle feed. The two areas have an identical polish and the differences in tool wear between them should be negligible. We found that the difference in surface quality varied with the direction of spindle feed in a very similar manner to what had been observed with the test grating and grism #1. Figure 12 illustrates the geometry of cutting with the two different directions of spindle feed.

With this new knowledge we cut grism #2 using the same direction of spindle feed as used to cut the test grating. Otherwise the machining parameters and procedures were the same as for grism #1. Tests showed that chipping of the vertical groove face was greatly reduced (see figure 13 for optical profilometry). We observed a diffraction pattern with a HeNe laser identical to grism #1 (i.e. no ghosts and nearly all the incident power diffracted into the second order). Unfortunately the surface error shown in figure 14 is considerably poorer measuring 0.389 wave P-V, 0.074 wave rms over the full aperture and 0.222 wave P-V, 0.043 wave rms over 80% of the full aperture. Grism #2 still met the requirement for rms surface error but slightly exceeded the peak to valley specification.

Between the cutting of grisms #1 and #2 another machining job had been done on PERL, which required the removal and reinstallation of the upper mounting plate of the translation stage, a one-inch thick steel plate with tapped holes that can be seen in the right side photo of figure 6. Because we rely on passive structural stability to maintain the critical distance between the tool and the grism blank, any shift in the vertical position of the mounting plate produces an equal shift in the vertical position of the groove. One can easily imagine submicron drifts over time as stresses in the mounting bolts securing the plate relax after the reinstallation.

An examination of the grism #2 interferogram showed that the dominant surface error was cylindrical in shape with the axis of the cylinder is parallel to the grooves. The deviations from planarity do not occur along a groove, which is cut on a time scale of minutes, but rather across a large number grooves, which take days to cut. The observed surface error is consistent with a slow drift in the vertical position of the mounting plate.

7. CONCLUSIONS AND FUTURE WORK

The optical performance of the ZnSe grisms met or exceeded requirements. Grism #1 will be installed in NIRISS in late 2014 at the same time that the detector array is upgraded/replaced. This activity will occur at NASA's Goddard Space Flight Center. Launch is tentatively scheduled for 2018. Grism #2 will be installed in an instrument simulator at the

Université de Montréal. It will be used to study the systematics of precision photometry with NIRISS.

In order to reduce the ~20% air-ZnSe reflection loss, an antireflection (AR) coating will be applied to the entrance face of the gratings. Some consideration was given to AR coating the grooves. Work at UT Austin with silicon gratings for the JWST NIRCcam demonstrated that a broadband (2.0-5.0 μm) antireflection coating can be deposited on a grating surface without significant degradation of performance¹⁰. An AR coating was applied to the grooves of the ZnSe test grating. Results will be reported in a companion paper¹¹.

Several things were learned during the course of this project. We confirmed on a full size grating that unidirectional cutting on our machine greatly reduces periodic error in groove position and the consequent ghosts. We observed a preferred direction of spindle feed relative to the shape of the tool for minimizing groove chipping. It was also observed that removing and reinstalling elements of the support structure can increase grating surface error, possibly until system stresses are fully relaxed.

ACKNOWLEDGEMENTS

Special thanks are due to Joe Galkowski whose guidance and encouragement kept this project moving forward to its successful completion. Thanks also to Marcia Kellam for the Zygo measurements of surface error. Lawrence Livermore National Laboratory is operated by Lawrence Livermore National Security, LLC, for the U.S. Department of Energy, National Nuclear Security Administration under Contract DE-AC52-07NA27344.

REFERENCES

- [1] Doyon, R. et al. ,”The JWST Fine Guidance Sensor (FGS) and Near-Infrared Imager and Slitless Spectrograph (NIRISS),” Proc. SPIE 8442, 84222R (2012).
- [2] Doyon, R. et al., “Status of the JWST near-infrared imager and slitless spectrograph (NIRISS),” Proc. SPIE 9143, (2014).
- [3] <http://www.stsci.edu/jwst/instruments/niriss/ObservationModes/soos>
- [4] Kuzmenko, P. J., Little, S. L., Little, L. M., Wilson, J. C., Skrutskie, M. F., Hinz, P. M., Leisenring, J. M. and Durney, O., “Fabrication and testing of germanium gratings for LMIRcam,” Proc. SPIE 8450, 84503P (2012).
- [5] Ikeda, Y., Kobayashi, N., Kuzmenko, P. J., Little, S. L., Yasui, C., Kondo, S., Mito, H., Nakanishi, K. and Saragaku, Y., “Fabrication and current optical performance of a large diamond-machined ZnSe immersion grating,” Proc. SPIE 7739, 77394G (2010).
- [6] Palmer, E. W. et al., “Diffraction gratings,” Reports on Progress in Physics 38, 975-1048 (1975).
- [7] Loewen, E. G. and Popov, E., [Diffraction Gratings and Applications], Dekker, New York, 420 (1997).
- [8] Ikeda, Y., unpublished (2012).
- [9] Li, H. H., ”Refractive Index of ZnS, ZnSe, and ZnTe and Its Wavelength and Temperature Derivatives,” Journal of Physical and Chemical Reference Data 13, 103-150 (1984).
- [10] Gully-Santiago, M., Wang, W., Deen, C., Kelly, D., Greene, T. P., Bacon, J. and Jaffe, D. T., “High Performance Silicon Gratings for 1.2-8.0 μm : Detailed Results from the JWST-NIRCcam Devices,” Proc. SPIE 7739, 77393S (2010).
- [11] Albert, L., Kuzmenko, P. J., Doyon, R., Little, S. L., and Enzor, G. S., “Space qualification of an anti reflection coating on the ruled surface of a ZnSe grating prism: increasing the throughput of the single-object slit-less spectroscopy mode of NIRISS onboard JWST,” Proc. SPIE 9151 (2014).

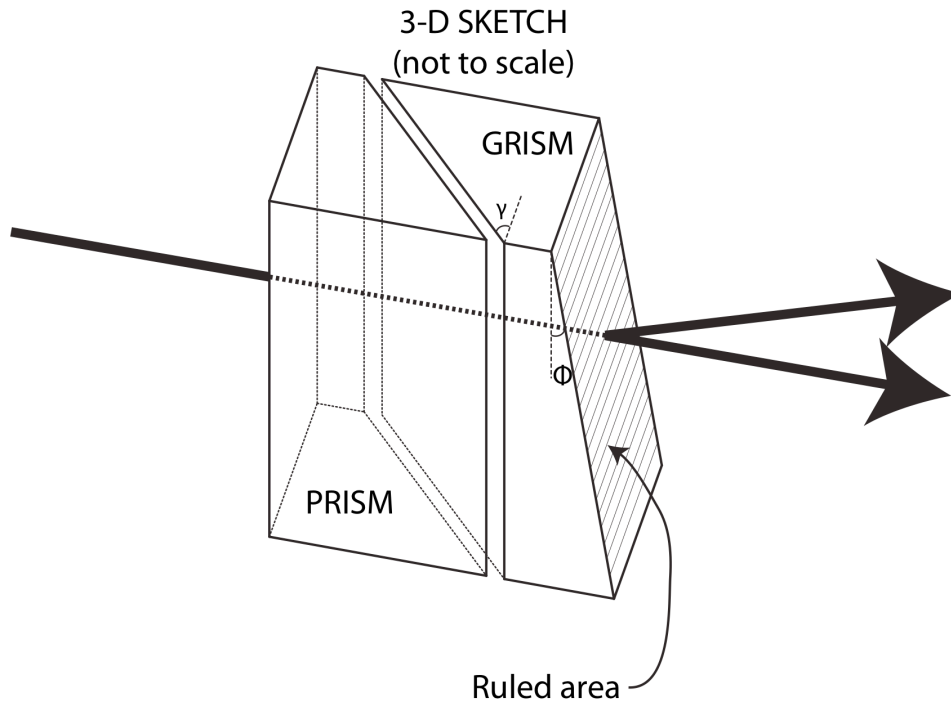


Figure 1. NIRISS optical path through GR700XD consisting of ZnSe grism and ZnS prism cross-disperser.

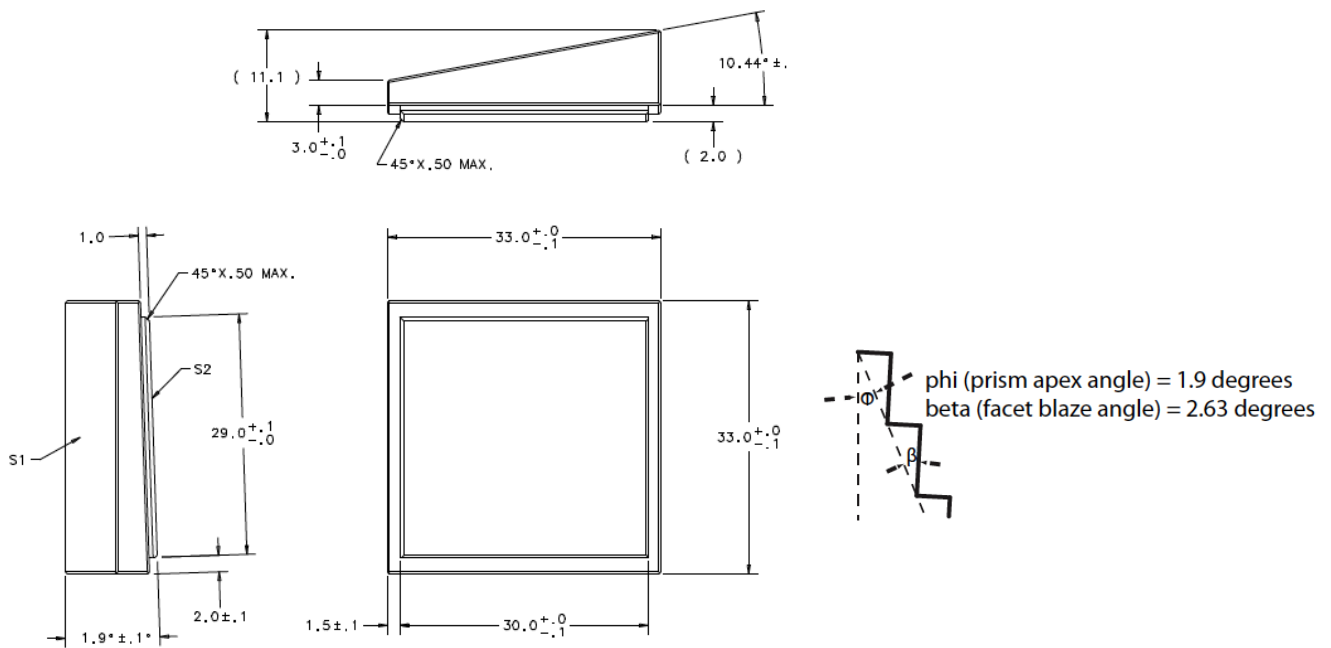


Figure 2. Drawing of ZnSe grism blank shows dimension and angles as well as details of the grating surface.

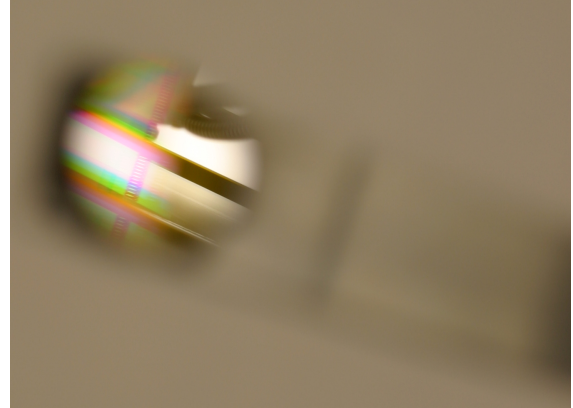
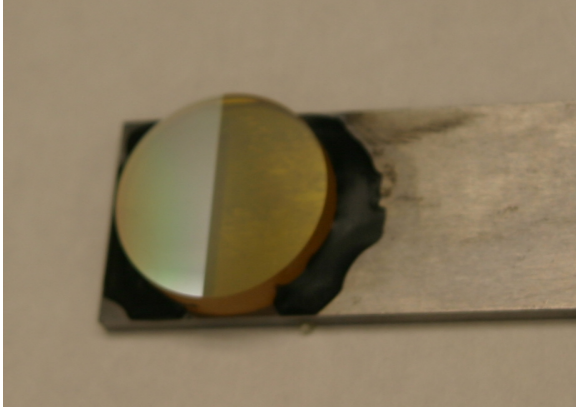


Figure 3. Left photo shows ZnSe ruling after removal from PERL. The grating covers the left half of the disc. In the right photo the focus is beyond the disc. Colored bands show diffraction of overhead fluorescent light.

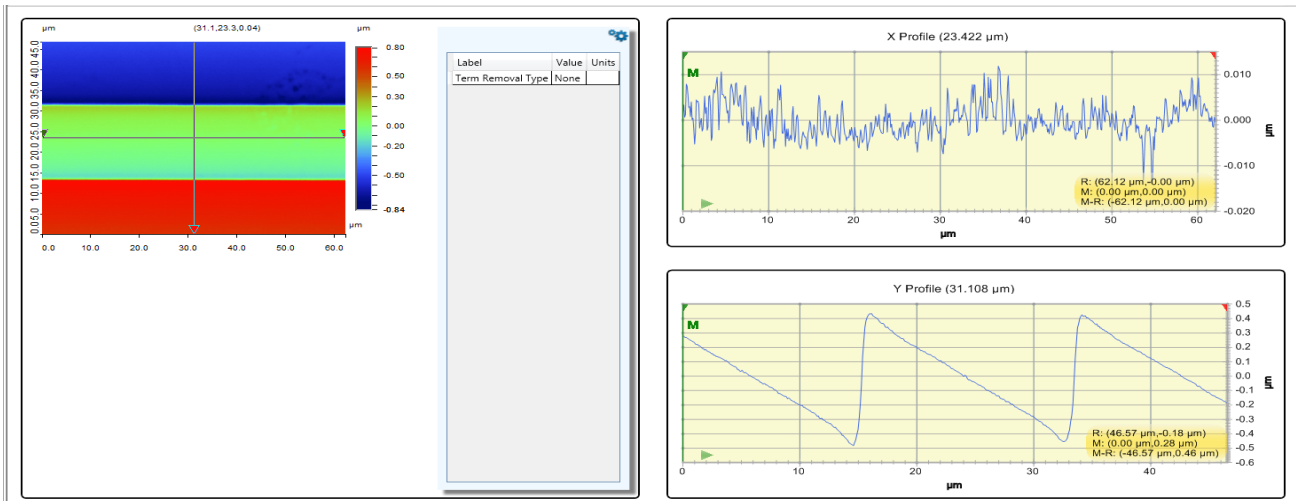


Figure 4. Optical profilometry of test grating on ZnSe disc displays 2D map of height plus profiles across and along grooves.

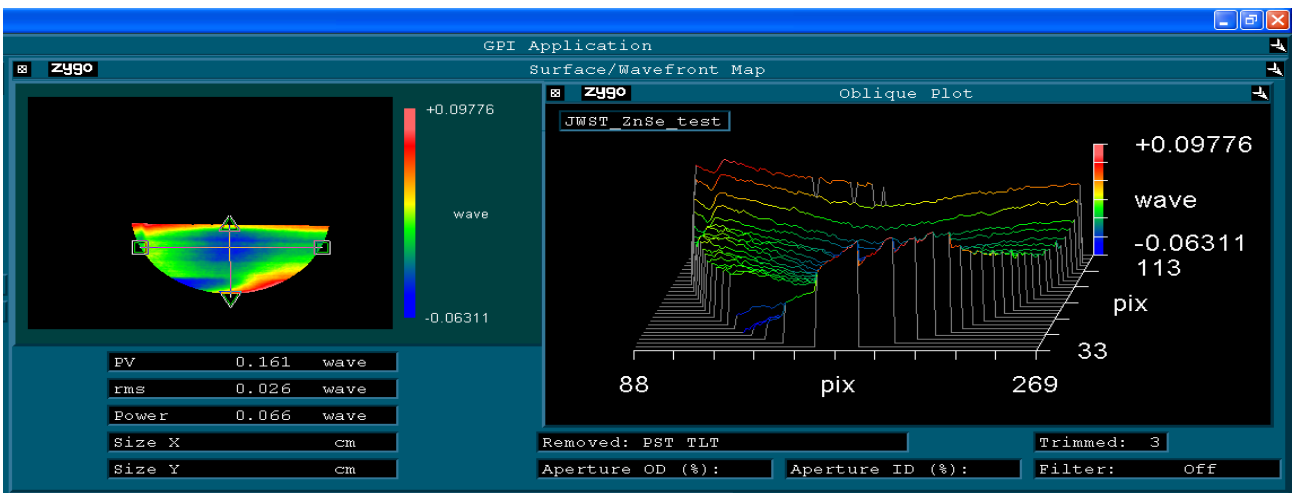


Figure 5. Interferometric measurement of surface error of the test grating on the ZnSe disc shows most of the error near the edges.

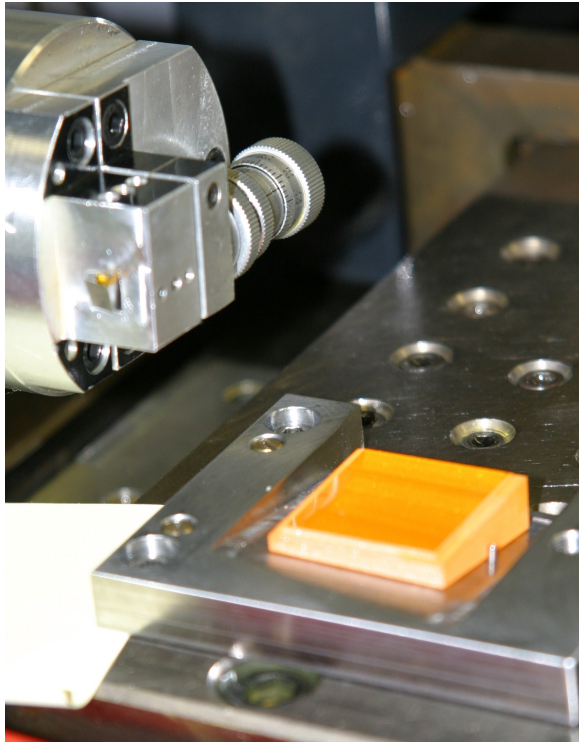


Figure 6. Grism #1 fixtured in PERL shown before (left) and after (right) machining.

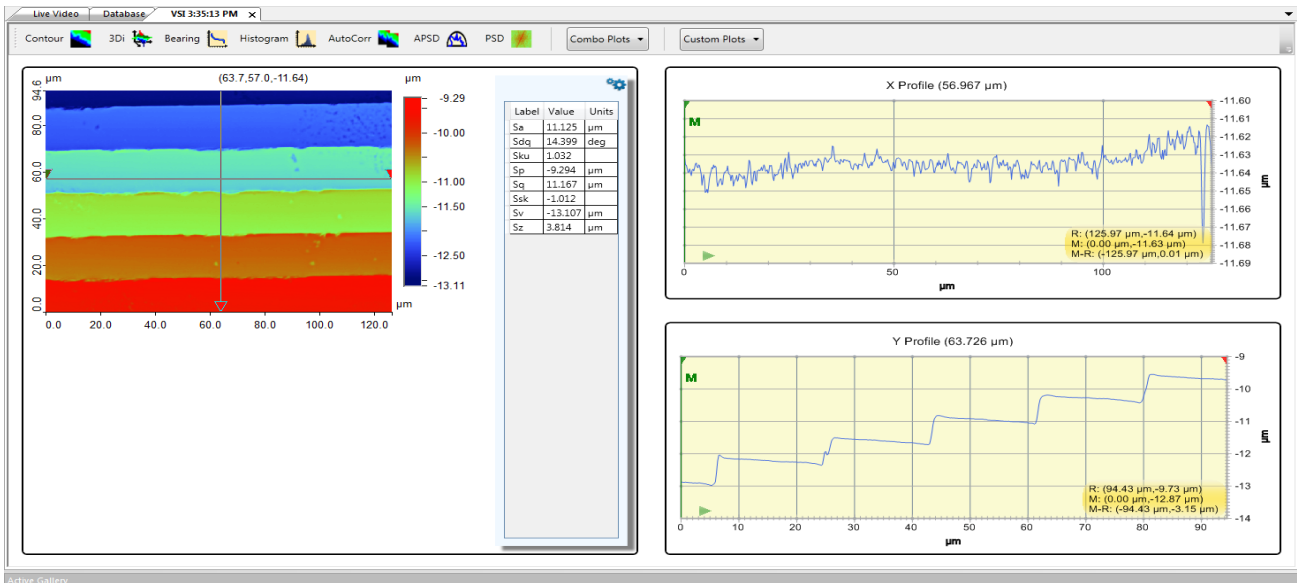


Figure 7. Veeco optical profilometer measurements were taken at nine locations across the surface of grism #1. The data shown above was taken from the middle of the grism. Some chipping and irregularities are seen on the vertical faces that were not observed in the test grating (figure 4), but the groove shapes are generally good and a roughness of only a few nm is seen on the facets.

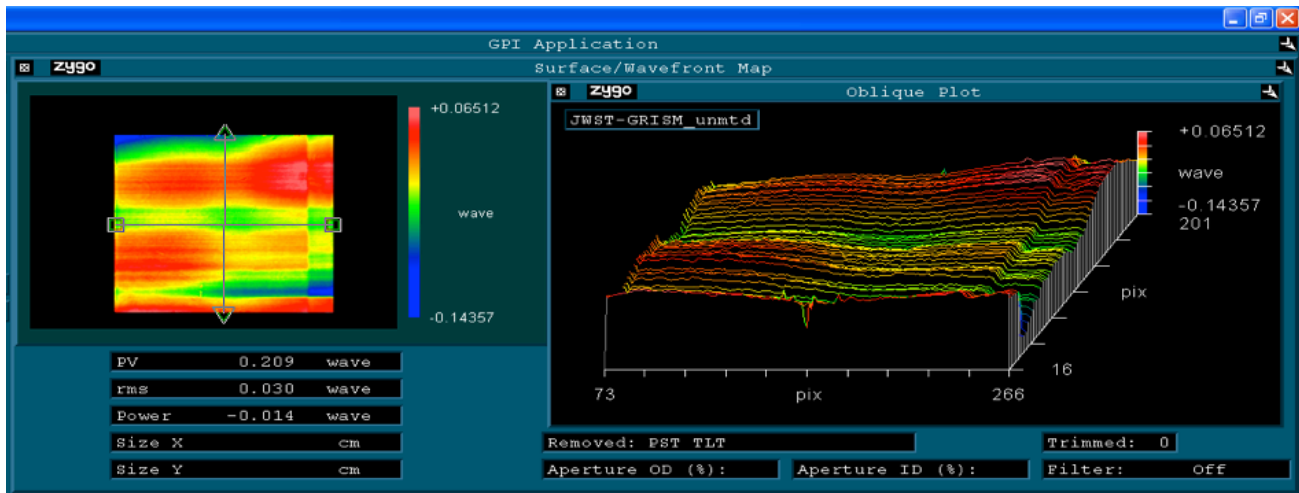


Figure 8. Interferometric measurement of surface error on grism #1 after removal from fixture and cleaning. Values of 0.209λ P-V and 0.030λ rms over the full aperture fall to 0.125λ P-V and 0.022λ rms over 80% aperture.

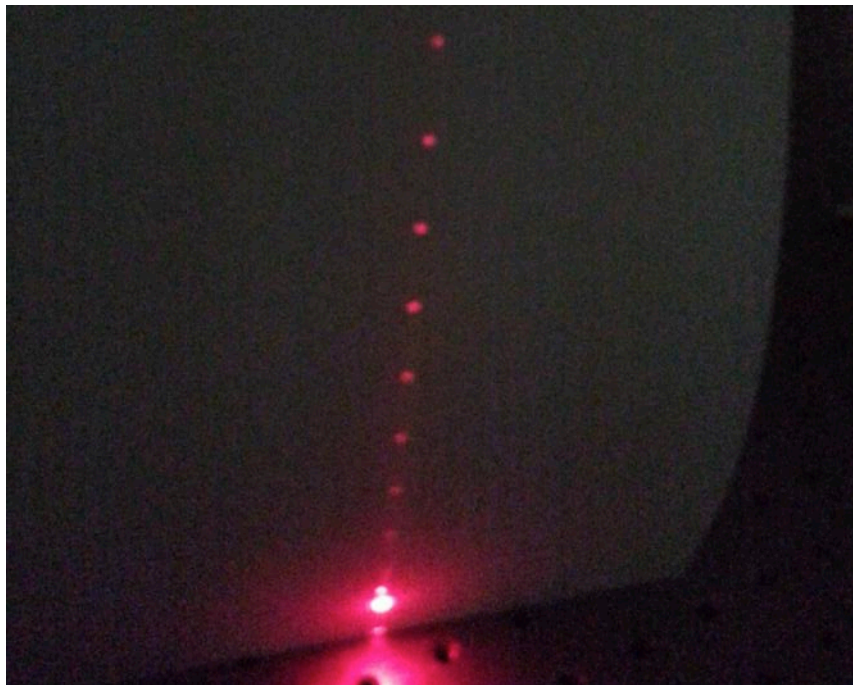


Figure 9. This diffraction pattern is produced by a HeNe laser transmitted through ZnSe grism #1. The very bright spot is second order diffraction demonstrating very high efficiency at 633 nm. Note the absence of inter-order ghosts or scatter.

PC Grate Model Transmission of the GR700XD (LLNL S/N#1)

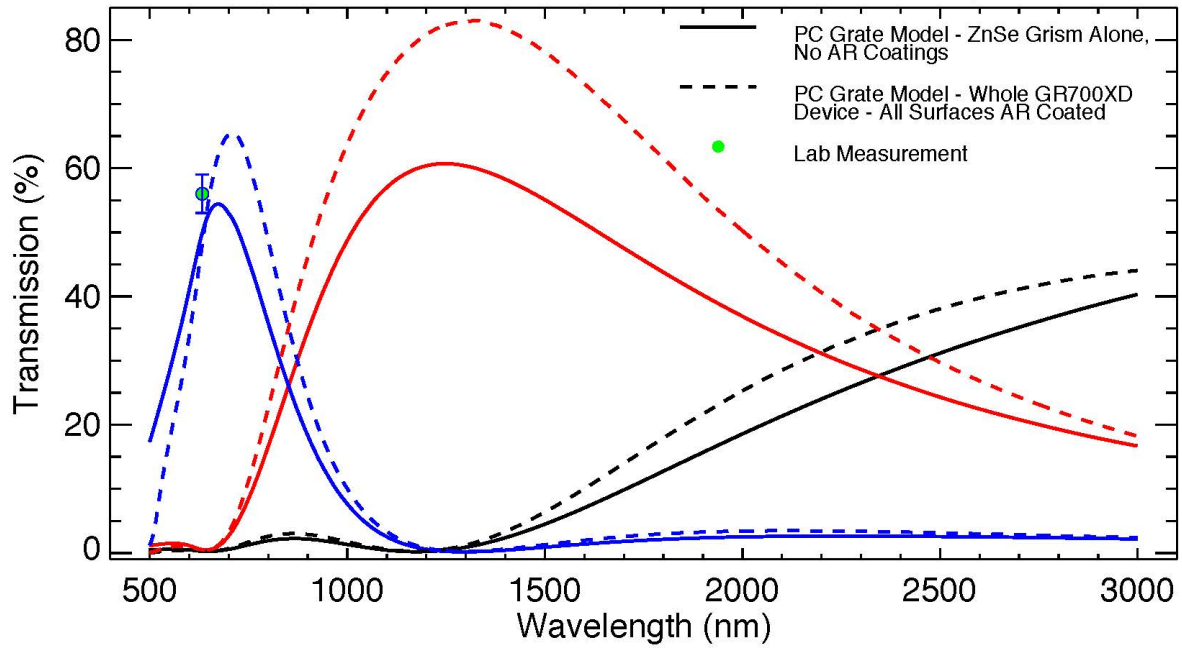


Figure 10. Each trace of the Y-profile on grism #1 (as shown in figure 7) covers 4 complete grooves. The program PCGrate was used to calculate the diffraction efficiency for each of the 4 grooves at each of 4 locations on the grism. These 16 curves of grism transmission vs. wavelength were then averaged together to produce the composite curve shown above. The solid line shows the results for an uncoated grism alone. A circle indicates the measured transmission of uncoated Grism #1 at 633 nm ($T=56\%$) using a 3 mm HeNe beam passing through the center of the grism. The dotted lines are results for the complete GR700XD with all surfaces AR coated. Diffraction order 0 is plotted in black, order 1 in red and order 2 in blue.

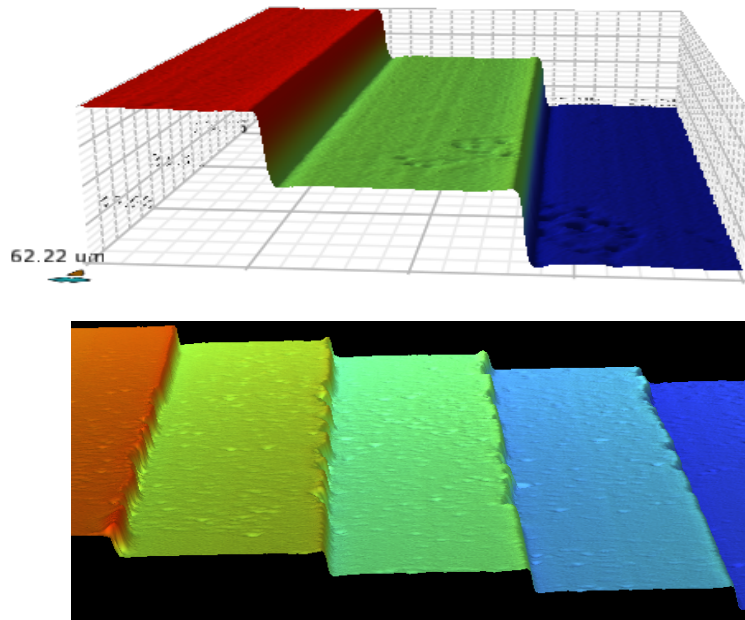


Figure 11. 3D plots of optical profilometry data were generated for the ZnSe test ruling (upper) and grism #1 (lower). The surfaces (especially the vertical ones) of grism #1 are rougher and there is more pronounced chipping at the corners of the grooves.

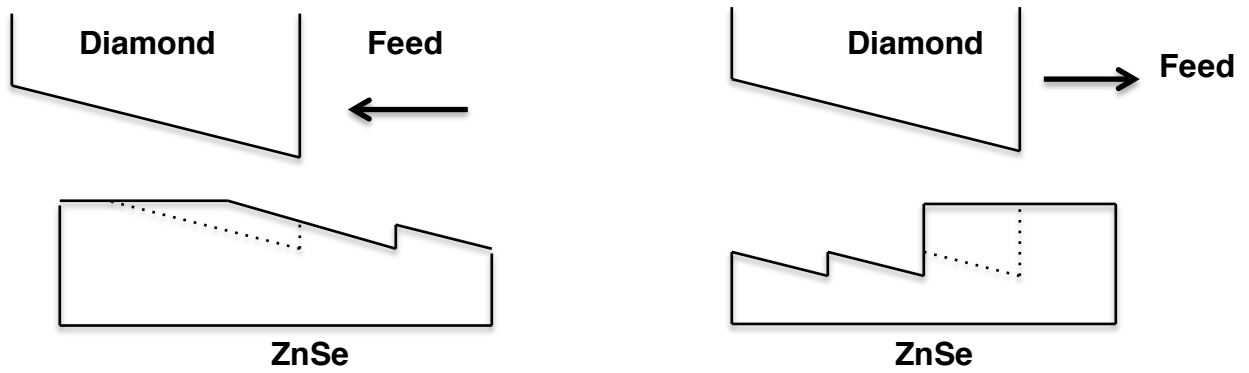


Figure 12. Graphic shows two possible directions of tool advancement to cut successive grooves. The tool feed shown at the left results in poorer facets and chipped groove edges. The one on the right produces cleaner grooves and reduced chipping.

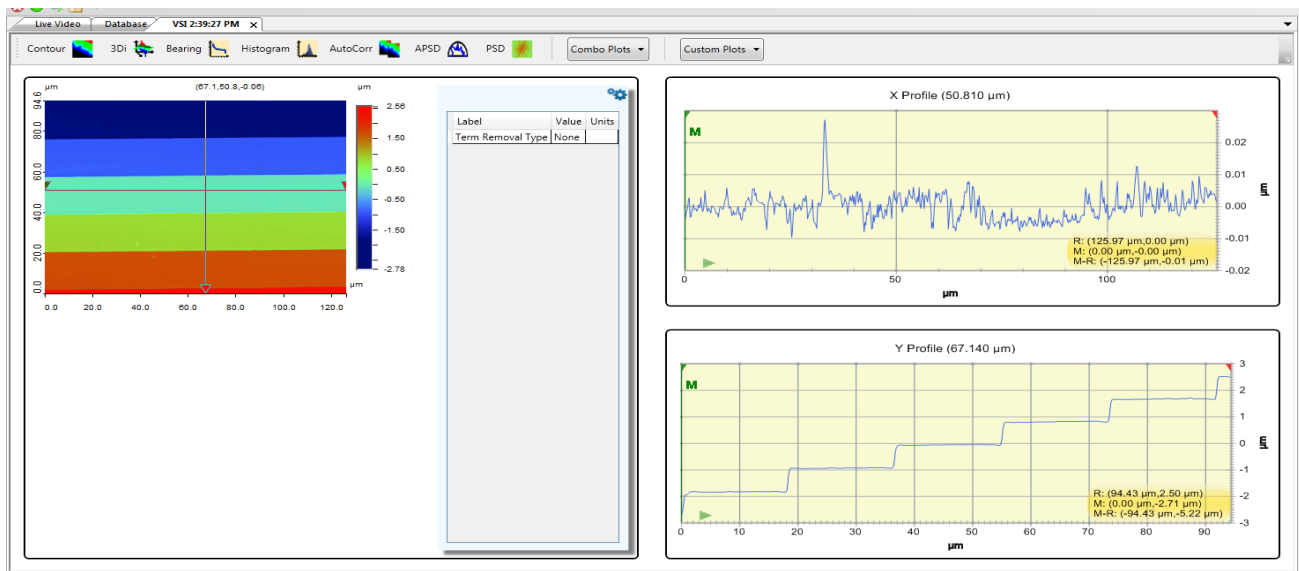


Figure 13. Veeco optical profilometer measurement on grism #2 shows cleaner grooves with less edge chipping than grism #1. Results are comparable to the test grating (see figure 4), which was cut with the same tool feed.

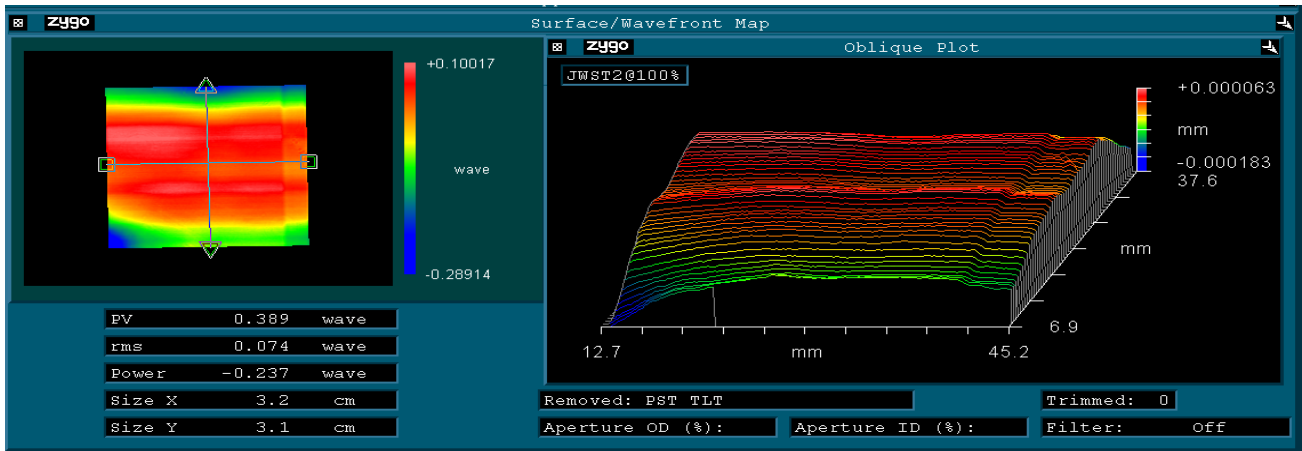


Figure 14. Measurement of surface error on grism #2 show a cylindrical shape with the axis aligned left to right, parallel to the grooves. Values of 0.389λ P-V and 0.074λ rms over the full aperture fall to 0.222λ P-V and 0.043λ rms over 80% aperture.